Enhanced photocatalytic activity of environment-friendly C/ZnFe$_2$O$_4$ nanocomposites: application in dye removal

Sunitha Salla[a,*], Nageswara Rao Ankem[a], Ponnusamy Senthil Kumar[b,*], A. Annam Renita[c], Kavin Micheal[d]

[a]Department of Chemistry, Sathyabama Institute of Science and Technology (Deemed to be University), Chennai 600119, India, Tel. +91 9940189810; emails: sunithasalla@gmail.com (S. Salla), nkemrao@rediffmail.com (N.R. Ankem)
[b]Department of Chemical Engineering, SSN College of Engineering, Kalavakkam, India, Tel. +91 9884823425; email: senthilchem8582@gmail.com
[c]Department of Chemical Engineering, Sathyabama Institute of Science and Technology (Deemed to be University), Chennai 600119, India, Tel. +91 7708710793; email: reniriana@gmail.com
[d]Research Department of Physics, Khadir Mohideen College, Adirampattinam 614701, India, email: kavinvasantha@gmail.com

ABSTRACT

A scheme toward enhancing the photocatalytic activity of ZnFe$_2$O$_4$ was achieved by shell coating of graphitic-mimic carbon stratum using solution combustion method. In the present study, the solution combustion method was used to synthesize carbon-doped zinc ferrite (C/ZnFe$_2$O$_4$) nano-composite. X-ray diffraction (XRD), Fourier transform infrared spectroscopy, field-emission scanning electron microscopy, energy-dispersive X-ray spectroscopy (EDAX), UV-vis diffuse reflection spectroscopy (UV-vis-DRS), and Brunauer–Emmet–Teller (BET) surface analyses were utilized to pinpoint the structure and morphological evolutions. The 2θ XRD spectra suggested that the nanocomposite consists of zinc oxide nanoparticles with zincite formation, and the mean crystallite dimension was established to be 6.49 nm. EDAX analysis confirmed the existence of elements like Fe, Zn, and O. UV-vis-DRS studies have shown bandgap of 3.14 eV. The surface area of the porous C/ZnFe$_2$O$_4$ was calculated to be 65 m^2 g^{-1} using BET experiment. The photocatalytic activities of C/ZnFe$_2$O$_4$ were investigated by the degradation of acid blue 113 (AB 113) under UV light irradiation. From the degradation studies, it was observed that C/ZnFe$_2$O$_4$ exhibited higher photocatalytic activity. The small size, high surface area, and synergistic effect in the C/ZnFe$_2$O$_4$ nanocomposite are responsible for high photocatalytic activity. The influence of various parameters such as the initial dye concentration, pH, and catalyst weight on the photocatalytic degradation of the dye was also investigated. The C/ZnFe$_2$O$_4$ nanocomposite is stable, easily separable, and reusable photocatalyst. Further, the possible photocatalytic degradation mechanism of AB 113 over C/ZnFe$_2$O$_4$ nanocomposite has been proposed.

Keywords: Acid blue 113; Photocatalytic degradation; Nanocomposites; Solution combustion; Kinetics

1. Introduction

In the current era, the nano-semiconductor intervened photocatalysis has acquired prominence in treating the wastewater generated from the various industries like paper, sugar, leather, textile, and dyeing. This sewerage effluvium contains a substantial quantity of organic pigments [1–3]. As soon as these organic adulterant toxins are released to the primary water bodies, they induce a multitude of harms both

* Corresponding authors.

to the neighborhood and environment [4,5]. Heterogeneous photocatalysis is considered to be a cost-effective management procedure for the detoxification of dye-containing sewerage water [6–10].

Along with the various identified treatment types, semiconductor heterogeneous photocatalysis is an adaptable, cost-viable, and green management method for the annihilation of organic pollutants in water. Invariably, photocatalysis involves the use of semiconductor metal oxides such as TiO_2, ZnO, Fe_2O_3, WO_3, and MnO_2 as photocatalysts [11–15]. Although TiO_2 was widely used, however, prevalent utilization of TiO_2 is not economical for mega-scale wastewater treatment process. ZnO is privileged due to its extraordinary photocatalytic bout and chemical constancy [9,16]. It has been a well-chronicled scientific fact that photocatalytic effectiveness of ZnO is superior or comparable to TiO_2.

At the present time, nanomaterials are of immense curiosity from the research explorations due to radical transformation of the material's properties upon attaining nanometer range particle size. While the particle size decreases, it dramatically increases the surface area to volume ratio and porosity, thus tremendously increasing photocatalytic activity. Other consequence is the enormous increase in the bandgap, thus changing the electrical and optical properties of the material and making the material suitable for newer applications and devices [17,18]. A large excitation binding energy of 60 meV and a wide bandgap of 3.37 eV make ZnO an excellent n-type semiconductor [19,20], due to which many researchers were fascinated toward the possible utilization of ZnO in innumerable photocatalytic reactions [21–24]. So, nano zinc oxide (ZnO) has been accepted as a capable photocatalyst due to low cost, ease of availability, high catalytic activity, and chemical stability [25–29].

In earlier studies, the photocatalytic activity of semiconductor nanoparticles could be improved (particularly in the UV spectral region) by impurity doping [30]. In continuation, the work presented here studied the effect of iron doping on Zn, emphasizing on photocatalysis and biological activity. Iron's ionic radius (0.064 nm) is similar to Zn (0.060 nm); hence, ease of doping was expected. Nanosized zinc ferrite ($ZnFe_2O_4$) has potential applications as sensors due to their electrical, magnetic, and photocatalytic capabilities [31–36]. Li et al. reported that nanotube arrays of $ZnFe_2O_4$ synthesized by sol-gel method exhibited improved photocatalytic activity of 4-chlorophenol under visible light [37]. Many researchers found that the enhanced activity of various nano $ZnFe_2O_4$ particles prepared by the hydrothermal process was attributed to structure with enormous surface area in contrast to massive particles of $ZnFe_2O_4$ [38]. Hence, it is crucial to develop a green method for the preparation of $ZnFe_2O_4$ nanoparticles. Several means are in routine to progress the photostability of ZnO. This comprises surface coating of ZnO with organic ligands [39] and hybridization of ZnO surface using fullerenes C_{60} and carbon [40,41]. In the abovementioned context, a variety of experiments have been performed to elevate the rate of photodegradation of ZnO by pairing adsorbents similar to activated carbon which make avail high concentration of goal substances in the region of the catalyst particulate [42–47].

In this work, an endeavour has been carried out to produce porous $C/ZnFe_2O_4$ nanocomposite by solution burning process that has the benefit of straight forwardness and swiftness. The $C/ZnFe_2O_4$ nanocomposite synthesized were characterized by various systematic techniques like X-ray diffraction (XRD), Fourier transformation infrared spectroscopy (FTIR), field-emission scanning electron microscope (FESEM), energy-dispersive X-ray spectroscopy (EDAX), UV diffuse reflection spectroscopy (DRS), and Brunauer–Emmet–Teller (BET) analyses to know about their surface and morphological structure. The degradation of Acid Blue 113 (AB 113) under UV light irradiation using batch reactor was utilized to examine the photocatalytic activity of $C/ZnFe_2O_4$ nanocomposite. The influence of various working parameters such as catalyst loading, effect of dye concentration, and consequence of pH was calculated methodically. The as prepared $C/ZnFe_2O_4$ nanocomposite was also institute superior antibacterial and anticancer activity.

2. Materials and methods

2.1. Materials

AB 113 marketed as navy blue S5R (C.I.No. 26360) sodium hydroxide pellets (NaOH) and hydrochloric acid (HCl) was acquired from SDFCL, India. Zinc nitrate hexahydrate $Zn(NO_3)_2 \cdot 6H_2O$, dextrose, glycine ($C_2H_5NO_2$), and ferric nitrate hydrate ($Fe(NO_3)_3 \cdot 9H_2O$) were procured from Merck. All materials were of research grade and used without further purification.

2.2. Synthesis of C/ZnFe₂O₄ nanocomposites

The $C/ZnFe_2O_4$ nanocomposite was synthesized by solution combustion method. $Zn(NO_3)_2 \cdot 6H_2O$ and $Fe(NO_3)_3 \cdot 9H_2O$ were used as oxidizers with glycine as a fuel and dextrose as the carbon source. The procedure for the synthesis of $C/ZnFe_2O_4$ nanocomposite was adopted and modified as mentioned in earlier report [48]. For instance, the stoichiometric amounts of $Fe(NO_3)_3 \cdot 9H_2O$ (4.0 g) and $Zn(NO_3)_2 \cdot 6H_2O$ (1.4 g), glycine (7.8 g), and 1.0 g of dextrose were dissolved in 60 mL of double-distilled water. Then the reaction solution was magnetically stirred well and subsequently heated at 90°C to evaporate the excess of water. Then the obtained sample was heated at 350°C for 1 h. The obtained final product was air cooled and crushed to get the fine powders of $C/ZnFe_2O_4$ nanocomposite.

2.3. Photo-irradiation reaction procedure

Photo-irradiation was carried out using a UV light bulb (6 W) with peak wavelength of 360 nm under batch reactor. The experiments were conducted by taking a 250 mL of pigment solution of the required concentration with an identified load of photocatalyst. Earlier to the irradiation, the suspension was magnetically stirred in the dark for 0.5 h to establish adsorption–desorption equilibrium. The air-equilibrated conditions of suspension were maintained before and throughout the irradiation. Further, the blend was irradiated with visible light and at regular intervals; a sample of 3 mL was withdrawn and centrifuged. The spectrophotometer

excited at 565 nm was used to measure concentration of the dye solution.

2.4. Characterization techniques

XRD was performed (Rigaku X-ray diffractometer, Japan) with Cu Kα radiation (λ = 0.15418 nm). The crystalline phase of $ZnFe_2O_4$ was identified by comparing with JCPDS card no. 22-1012. FTIR studies were performed (Perkin Elmer System one FTIR). The FESEM and EDAX photographs of $C/ZnFe_2O_4$ nanocomposite were obtained using a field-emission scanning electron microscope (Carlzeiss, Supra 55, Germany). UV-vis studies were carried out using SL-210 UV-visible double-beam spectrophotometer. BET surface analysis was examined from the N2-adsorption isotherm via NOVA 2200*e* analyzer (Quantachrome Instruments, USA).

3. Results and Discussion

3.1. XRD studies

The XRD patterns of the synthesized $C/ZnFe_2O_4$ nanocomposite are shown in Fig. 1. It is obviously seen that almost all the diffraction peaks of $C/ZnFe_2O_4$ can be assigned to cubic phase of $ZnFe_2O_4$ (JCPDS 22-1012). The diffraction peaks at 2θ values of 18.4°, 29.9°, 35.2°, 42.7°, 53.1°, 56.5°, 62.3°, and 73.6° can be indexed to (111), (220), (311), (400), (422), (511), (440), and (533), which were well matched with the crystal planes of cubic $ZnFe_2O_4$, respectively. It was noticed that the diffraction patterns of $ZnFe_2O_4$ were not changed by addition of carbon with no particular diffraction peaks of carbon in the $C/ZnFe_2O_4$ composite, which might be because of low amount of carbon present in the composite and thick covering of $ZnFe_2O_4$ on the surface of carbon [49]. The estimated average crystallite size of the synthesized $C/ZnFe_2O_4$ nanocomposite using Debye-Sherrer's equation was found to be around 6.49 nm.
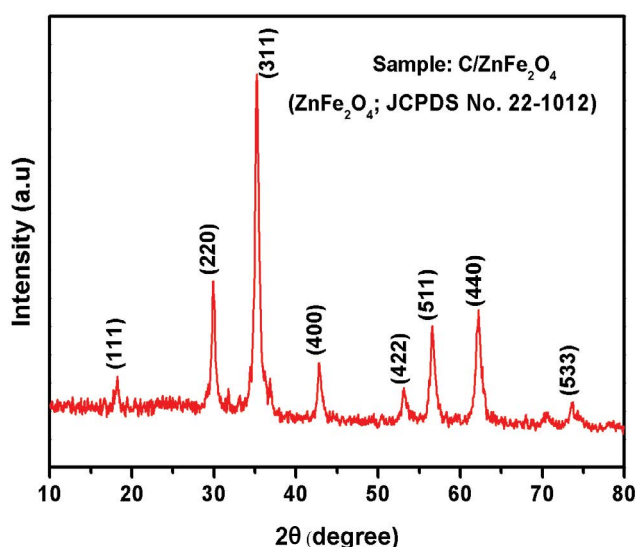
3.2. FTIR studies

The FTIR spectrum of the synthesized $C/ZnFe_2O_4$ nanocomposite sample is displayed in Fig. 2. It is a well-known technique to study the information on chemical structure and bonding [50–54]. In the FTIR spectrum of $C/ZnFe_2O_4$, the broad absorbance peaks from wave numbers 3,400–3,900 cm^{-1} and another sharp peak around 1,600 cm^{-1} were assigned to O–H stretching and O–H bending vibrations, respectively [55–57]. The absorption peaks in the range of 400–700 cm^{-1} could be attributed to the ZnO stretching modes. The main peaks were observed in the range of 1,100–1,600 cm^{-1} corresponding to the Zn–OH bending mode. The band peak at 1,378 cm^{-1} was attributed by C–OH bending vibrations. The peaks from 400 to 600 cm^{-1} are attributed to the bond between iron and oxygen (Fe–O). The obtained FTIR confirms the existence of carbon in $ZnFe_2O_4$ samples.

3.3. Surface morphology and elemental studies

The shape and surface morphology of the synthesized $C/ZnFe_2O_4$ nanocomposite were analyzed using FESEM. The FESEM image reveals that the entire product is having sponge-like agglomerate structure with a pore size of about 17.63 nm (Fig. 3(a)). The formation of sponge-like structures might be due to the sustained release of gas during the combustion process that promotes the formation of porous structure and rough surface, which is a unique characteristic of samples synthesized by the solution combustion method [48]. The good surface morphology of $C/ZnFe_2O_4$ nanocomposite was beneficial for an efficient separation of photoexcited electron–hole pair. Thus, the $C/ZnFe_2O_4$ nanocomposite would be expected to be an efficient material for photocatalytic degradation of AB 113. Further, the elemental composition of the prepared $C/ZnFe_2O_4$ sample was ascertained by EDAX analysis, and the corresponding results are displayed in Fig. 3(b). The EDAX studies of $C/ZnFe_2O_4$ nanocomposite confirm the presence of Zn, Fe, O, and C atoms, and no other impurities were found.
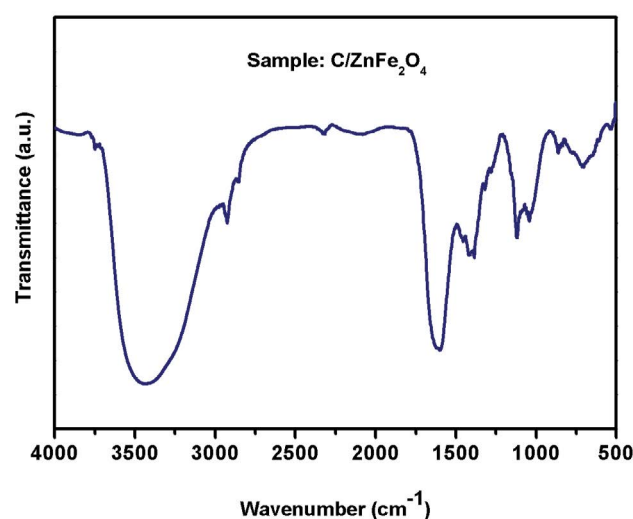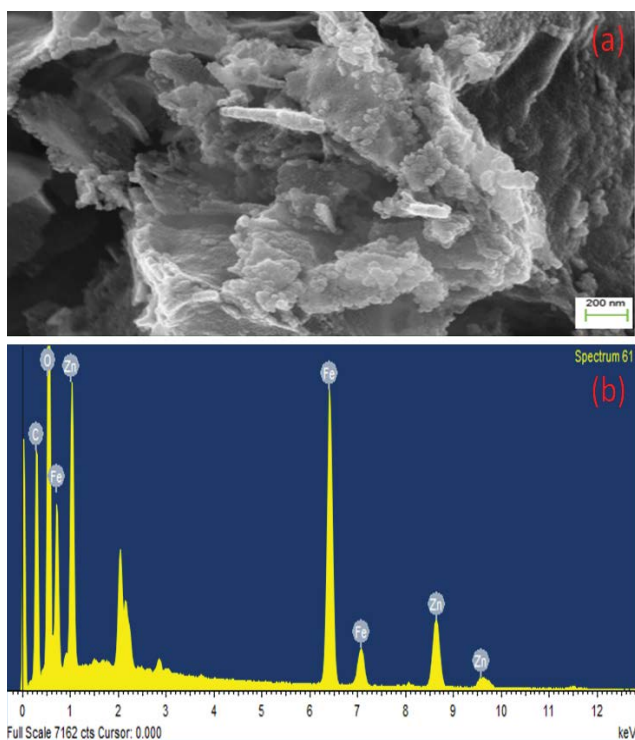

Fig. 1. XRD pattern of $C/ZnFe_2O_4$ nanocomposite.

Fig. 2. FTIR pattern of $C/ZnFe_2O_4$ nanocomposite.

Fig. 3. (a) FESEM images and (b) EDAX spectrum of C/ZnFe$_2$O$_4$ nanocomposite.

3.4. UV-vis DRS and BET analyses

The UV-vis DRS studies of the synthesized C/ZnFe$_2$O$_4$ nanocomposite sample were carried out to know the light absorption properties and the resultant characteristic spectra and are presented in Fig. 4(a). It can be observed that the absorption edge for the synthesized C/ZnFe$_2$O$_4$ was found to be at 394 nm, and the calculated band energy gap value is 3.14 eV. This absorption study shows that the C/ZnFe$_2$O$_4$ sample can absorb the light in the UV region to generate electron–hole pairs and thus prompt high photocatalytic performance of the C/ZnFe$_2$O$_4$ sample. Further, the specific surface area is also an important microstructural parameter of C/ZnFe$_2$O$_4$ nanocomposite, which depends on the geometrical shape and porosity of the particles. As a result, the observed specific surface area was found to be 65 m^2/g. The exhibited BET isotherm of C/ZnFe$_2$O$_4$ nanocomposite is displayed in Fig. 4(b).

3.5. Kinetics and photodegradation studies of AB 113

The photocatalytic degradation of the AB 113 dye over synthesized C/ZnFe$_2$O$_4$ nanocomposite has been carried out in the presence of UV light. The experimental data are given in Table 1, and the plot of photodegradation as a function of time is shown in Fig. 5. The stable nature of the AB 113 dye was clear from the blank test without photocatalyst. There was no noteworthy change in the initial concentration of AB 113 under an illumination of UV light for 100 min (Fig. 5(a)). Additionally, adsorption properties of AB 113 dye on the C/ZnFe$_2$O$_4$ photocatalyst were investigated in the
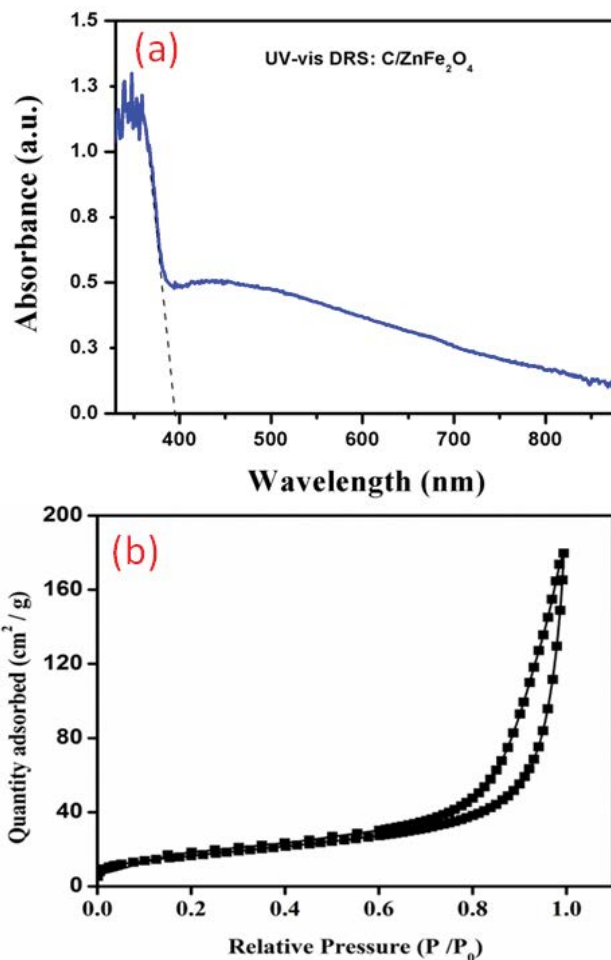

Fig. 4. (a) UV-vis DRS and (b) BET isotherm of C/ZnFe$_2$O$_4$ nanocomposite sample.

dark, and it was noticed that the adsorption equilibrium of the AB 113 dye in the C/ZnFe$_2$O$_4$ photocatalyst was achieved after 60 min (results not shown). Fig. 5(c) shows the complete degradation of AB 113 dye over 0.5 g/L of C/ZnFe$_2$O$_4$ nanocomposite under UV light irradiation for 100 min.

The photocatalytic degradation of AB 113 has been carried out at different pH values ranging from 6 to 8 (Fig. 6(a)). Fig. 6(a) shows the amendment of photodegradation of the dye as a function of time. The range of the initial rate is 0.44–1.85 μm/m. The optimum pH has been found to be 6.5. The effect of photocatalyst weight on the photodegradation of the dye has been studied in the range of 0.25–1.0 g/L. Fig. 6(b) shows the photodegradation of the dye at various catalyst weights. The optimal weight of the catalyst loading has been found to be 0.5 g/L. It was observed that the efficiency of the photocatalytic degradation increases with a photocatalyst loading up to 0.5 g/L, which might be because of an expansion in the amount of photon adsorbed. In addition, the accessibility of active sites on the photocatalyst surface was also increased, and it subsequently enhanced the photodegradation efficiency. Further, increasing the amount of C/ZnFe$_2$O$_4$, the photodegradation efficiency was decreased, which was because

Table 1
Photodegradability of AB 113

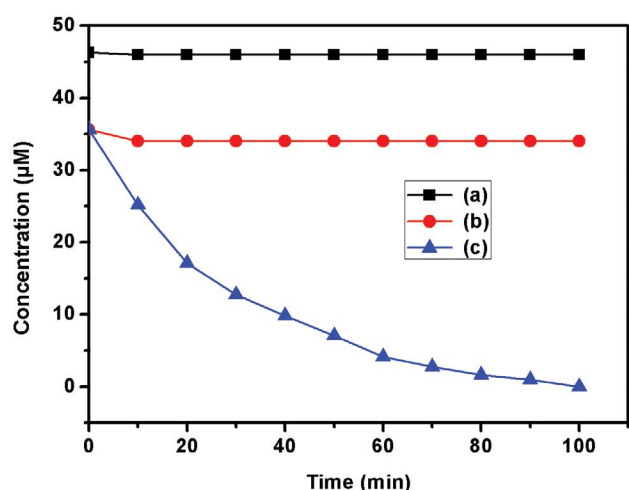| Time (min)	Concentration of the dye in μm		
	(a) Absence of photocatalyst	(b) In dark (0.5 g/L of C/ZnFe$_2$O$_4$)	(c) In UV light (0.5 g/L of C/ZnFe$_2$O$_4$)
Before adsorption	50.0	50.0	50.0
0	46.3	35.64	35.59
10	46	34	25.19
20	46	34	17.12
30	46	34	12.75
40	46	34	9.84
50	46	34	7.09
60	46	34	4.14
70	46	34	2.75
80	46	34	1.628
90	46	34	0.98
100	46	34	0

Fig. 5. Photodegradability of AB 113, (a) absence of photocatalyst, (b) 0.5 g/L of C/ZnFe$_2$O$_4$ nanocomposite in dark, and (c) irradiated with UV light in the presence of 0.5 g/L of C/ZnFe$_2$O$_4$ nanocomposite.

at high amount of C/ZnFe$_2$O$_4$ it might act as a charge recombination center.

The photocatalytic degradation of AB 113 has been carried out at different initial concentrations ranging from 25 to 150 μm. The variation of photodegradation as a function of time is shown in Fig. 6(c). There is an increase in the rate of photodegradation of the dye with an increase in concentration of the dye in the range of 25–50 μm. The reaction kinetics of the photocatalytic degradation of AB 113 over C/ZnFe$_2$O$_4$ nanocomposite was studied. The obtained results of the photocatalytic degradation of AB 113 were fitted by a pseudo-first-order kinetic equation.
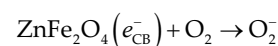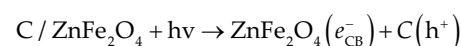
$$\ln\frac{C_0}{C} = k_{ap}t \qquad (1)$$

where C_0 is the initial concentration of AB 113, C is the concentration of AB 113 at regular time intervals, k_{ap} is the apparent pseudo-first-order rate constant (min^{-1}), and t is the light irradiation time [58]. The linear plot of log C_0/C vs. time obtained for various initial concentrations of the dye is shown in Fig. 7. It confirms the reaction to follow pseudo-first-order kinetics at concentrations employed in the study, and the rate constant of 0.00712 ± 0.0003 min^{-1} was observed for C/ZnFe$_2$O$_4$.

3.6. Photocatalytic degradation mechanism

The possible reaction mechanism diagram for the degradation of AB 113 using C/ZnFe$_2$O$_4$ photocatalyst under UV light is proposed in Fig. 8. Upon UV light illumination, the photogenerated electrons could be excited from the valence band (VB) to the conduction band (CB) of ZnFe$_2$O$_4$ by creating holes on the VB. Without carbon, the majority of electron–hole pairs rapidly recombine and just few electrons can be caught by O$_2$ to create •O$_2^-$ or caught by Fe^{3+}. Because of the presence of carbon in C/ZnFe$_2$O$_4$ nanocomposite, the photoinduced electrons on the CB of ZnFe$_2$O$_4$ can be transferred to the carbon because of their fantastic electronic conductivity. The transferred electrons gathered on the carbon were trapped by the adsorbed O$_2$ on the ZnFe$_2$O$_4$ surface to form •O$_2^-$. As a result, the recombination of electron–hole pairs was diminished and thus improved the charge separation, which results in the high photodegradation activity of C/ZnFe$_2$O$_4$ nanocomposite.

The possible photocatalytic degradation reactions of C/ZnFe$_2$O$_4$ are as follows:

$$C/ZnFe_2O_4 + h\nu \rightarrow ZnFe_2O_4\left(e_{CB}^-\right) + C\left(h^+\right)$$

$$ZnFe_2O_4\left(e_{CB}^-\right) + O_2 \rightarrow O_2^-$$

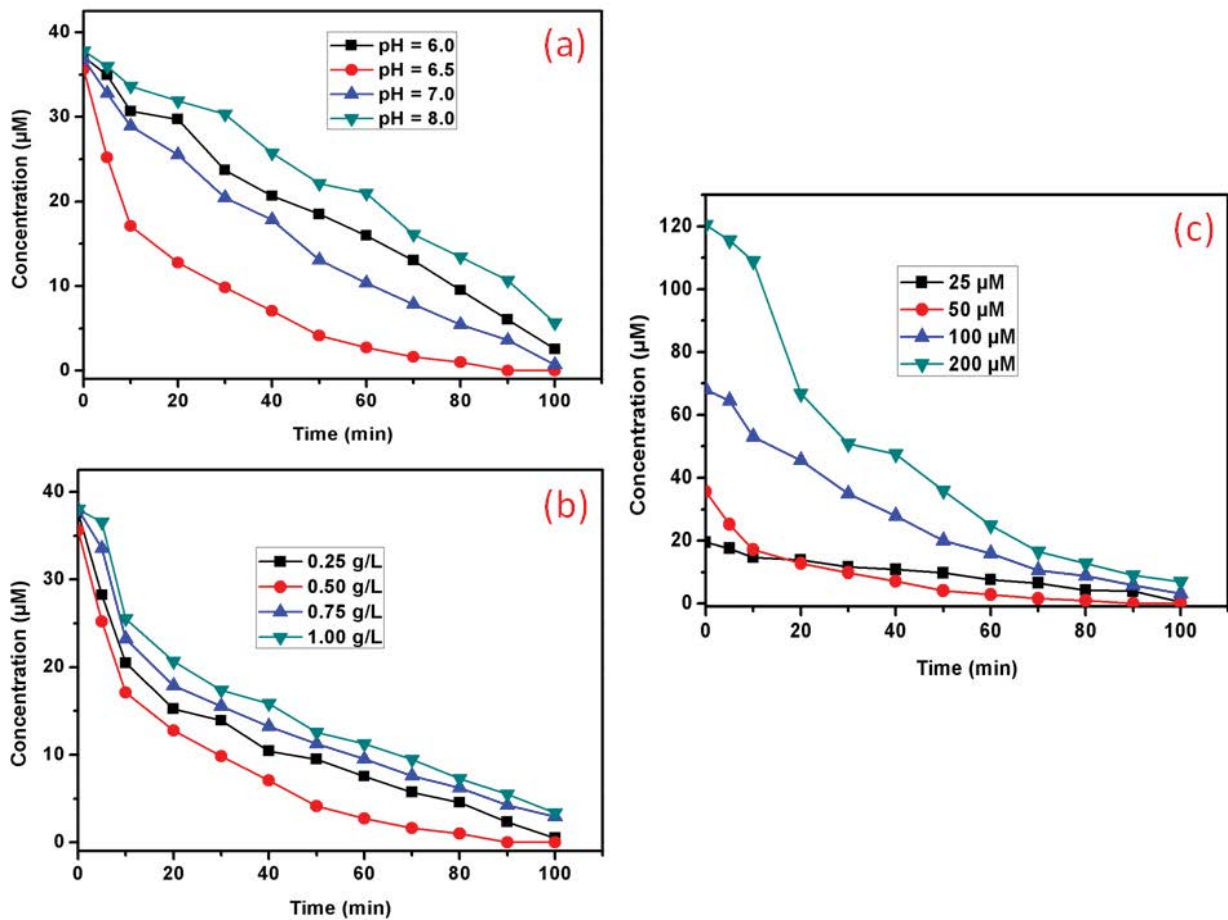$$O_2^- + 2\,e_{CB}^- + 2H^+ \rightarrow {}^\bullet OH + OH^-$$

Fig. 6. (a) Effect of pH, (b) catalyst loading, and (c) effect of initial dye on the photocatalytic degradation of AB 113.

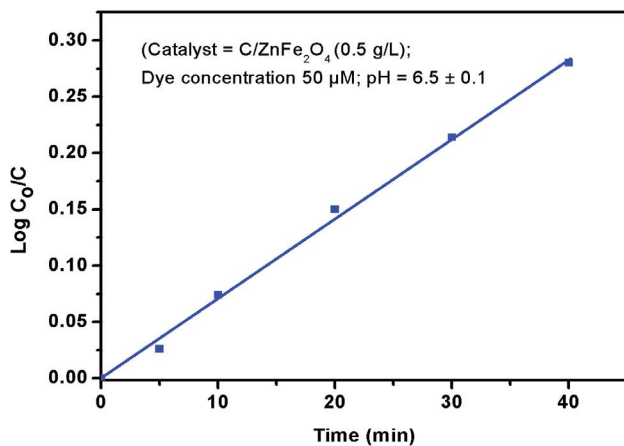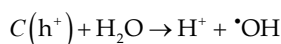Fig. 7. Pseudo-first-order kinetics plot of Log C_0/C versus time for AB 113.

$$C(h^+) + H_2O \rightarrow H^+ + {}^{\bullet}OH$$

$$AB\ 113 + {}^{\bullet}OH \rightarrow \text{oxidation products (CO}_2, H_2O \text{ etc).}$$

3.7. Comparative study

Ferrites are a group of materials with great potential in photocatalysis and possess excellent properties such as small bandgaps, stable structures, and low cost, and it is found to be a good photocatalyst for degradation of contaminants. A comparative study of $C/ZnFe_2O_4$ was performed using literature survey. A single-phase $ZnFe_2O_4$ was obtained in the temperature range of around 900°C–1,200°C using solid-state reaction method and possesses an average size of 51.9 nm with a bandgap of 1.90 eV [59]. The photocatalytic activity of these particles was investigated using the photodecomposition of isopropyl alcohol (IPA) under visible light (≥420 nm) and predicted to be much higher than that of the well-known nano TiO_2 photocatalyst. The synergistic action of ferrites with common oxidants including hydrogen peroxide (H_2O_2), peroxymonosulfate (PMS), and peroxydisulfate (PDS) in decomposing pollutants was also investigated [60].

The various ferrites, incorporated with various cations (MFe_2O_4, M = Ni, Co, Zn, and Sr), are utilized to modify the well-aligned TiO_2 nanorod arrays (NRAs), which are synthesized by hydrothermal method [61]. It is found that all MFe_2O_4/TiO_2 NRAs show obvious red shift into the visible light region compared with the TiO_2 NRAs. In particular, $NiFe_2O_4$ modification is demonstrated to be the best way
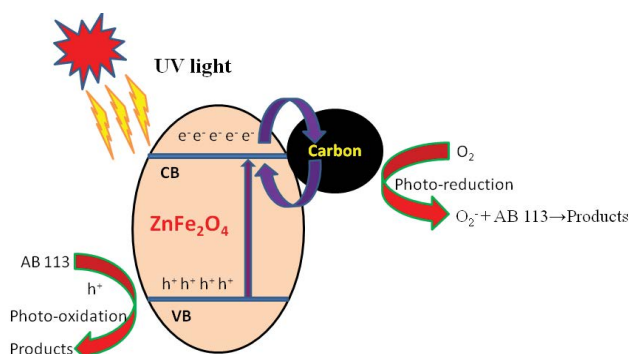
Fig. 8. Schematic view of the photocatalytic separation and transfer of photoinduced charges on the C/ZnFe$_2$O$_4$ photocatalyst under UV light.

to enhance the photoelectrochemical and photocatalytic activity of TiO$_2$ NRAs. Barium (II)-doped zinc ferrite/reduced graphene oxide (Ba^{2+}-ZF/rGO) was prepared using a one-step solvothermal method and used as magnetic nanohybrid adsorbents [62]. Ba^{2+}-ZF-rGO nanohybrid with an rGO content was used as an adsorbent and possesses excellent adsorption capacities for methylene blue at different initial concentrations, and the adsorption kinetics are described by the pseudo-second-order kinetic model.

4. Conclusions

In this research, the solution combustion method was used successfully to synthesize C/ZnFe$_2$O$_4$ nanocomposite. The powder XRD results confirmed that the synthesized nanocomposite exhibits zincite structure with average crystallite size of 6.49 nm. The bandgap energy value shows the emission of radiation in the UV region. The synthesized C/ZnFe$_2$O$_4$ nanocomposite was utilized for the photocatalytic degradation of AB 113. The optimum condition for higher photocatalytic degradation using C/ZnFe$_2$O$_4$ nanocomposite shows pH as 6.0, and optimum catalyst loading was found to be 0.5 g/L. The degradation of the dyes followed pseudo-first-order kinetics. The carbon coating was proven to be a promising approach to develop highly efficient, easily separable, and stable ZnFe$_2$O$_4$.

Finally, the possible mechanism for the photodegradation of AB 113 over C/ZnFe$_2$O$_4$ nanocomposite has been proposed.

References

[1] S.M. Ali, S.Z. Sabae, M. Fayez, M. Monib, N.A. Hegazi, The influence of agro-industrial effluents on River Nile pollution, J. Adv. Res., 2 (2011) 85–95.

[2] I.M. Ismail, A.S. Fawzy, N.M. Abdel-Monem, M.H. Mahmoud, M.A. El-Halwany, Combined coagulation flocculation pre-treatment unit for municipal wastewater, J. Adv. Res., 3 (2012) 331–336.

[3] M.M. Rushdi, El-Kilani, M.H. Belal, Modelling an environmental pollutant transport from the stacks to and through the soil, J. Adv. Res., 1 (2010) 243–253.

[4] C. Helmes, C.I. Tucker, Disperse blue 79 Environmental safety and human health effects of this commercially significant dye, Text. Chem. Color., 25 (1993) 15–17.

[5] M.M. Alnuaimi, M.A. Rauf, S.S. Ashraf, Comparative decoloration study of neutral red by different oxidative processes, Dyes Pigm., 72 (2007) 367–371.

[6] M. Kaneko, I. Okura, Application to environmental cleaning, Photocatalysis: Sci. Technol., 4 (2002) 109–184.

[7] M.N. Chong, B. Jin, C.W.K. Chow, C. Saint, Recent developments in photocatalytic water treatment technology: a review, Water Res., 44 (2010) 2997–3027.

[8] E. Forgas, T. Cserhati, G. Oros, Removal of synthetic dyes from wastewater: a Review, Environ. Int., 30 (2004) 953–971.

[9] M.R. Hoffmann, S.T. Martin, W. Choi, D.W. Bahnemann, Environmental applications of semiconductor photocatalysis, Chem. Rev., 95 (1995) 69–96.

[10] K. Hashimoto, H. Irie, A. Fujishima, TiO$_2$ photocatalysis: a historical overview and future prospects, Jpn. J. Appl. Phys., 44 (2005) 8269–8285.

[11] S.K. Kansal, M. Singh, D. Sud, Studies on photodegradation of two commercial dyes in aqueous phase using different photocatalysts, J. Hazard. Mater., 141 (2007) 581–590.

[12] C.A.K. Gouvea, F. Wypych, S.G. Moraes, N. Duran, N. Nagata, P.P. Zamora, Semiconductor-assisted photocatalytic degradation of reactive dyes in aqueous solution, Chemosphere, 40 (2000) 433–440.

[13] B. Neppolian, H.C. Choi, S. Sakthivel, A. Banumathi, V. Murugesan, Solar/UV-induced photocatalytic degradation of three commercial textile dyes, J. Hazard. Mater., 89 (2002) 303–317.

[14] I.M. Szilagyi, B. Forizs, O. Rosseler, A. Szegedi, P. Nemeth, P. Kiraly, G. Tarkanyi, B. Vajna, K. Varga-Josepovits, K. Laszlo, A.L. Toth, P. Baranyai, M. Leskela, WO$_3$ photocatalysts: influence of structure and composition, J. Catal., 294 (2012) 119–127.

[15] A. Rajat, V. Jitendra, P.B. Punjabi, S.C. Ameta, Use of semiconducting iron(III) oxide in photocatalytic bleaching of some dyes, Indian J. Chem. Technol., 13 (2006) 114–118.

[16] R.M. Alberici, W.F. Jardim, Photocatalytic destruction of VOCs in the gas-phase using titanium dioxide, Appl. Catal. B: Environ., 14 (1997) 55–68.

[17] G. Sivalingam, K. Nagaveni, M.S. Hegde, M. Giridhar, Photocatalytic degradation of various dyes by combustion synthesized nano anatase TiO$_2$, Appl. Catal. B: Environ., 45 (2003) 23–38.

[18] L. Junping, X. Yao, L. Yong, W. Dong, S. Yuhan, Synthesis of hydrophilic ZnS nanocrystals and their application in photocatalytic degradation of dye pollutants, China Particuol., 2 (2004) 266–269.

[19] S. Suwanboon, P. Amornpitoksuk, A. Haidoux, J.C. Tedena, Structural and optical properties of undoped and aluminium doped zinc oxide nanoparticles via precipitation method at low temperature, J. Alloys Compd., 462 (2008) 335–339.

[20] P. Zu, Z.K. Tang, G.K.L. Wong, M. Kawasaki, A. Ohtomo, K. Koinuma, Y. Sagawa, Ultraviolet spontaneous and stimulated emissions from ZnO microcrystalline thin films at room temperature, Solid State Commun., 103 (1997) 459–463.

[21] M.L. Curri, R. Comparelli, P.D. Cozzoli, G. Mascolo, A. Agostiano, Colloidal oxide nanoparticles for the photocatalytic degradation of organic dye, Mater. Sci. Eng., 23 (2003) 285–289.

[22] M. Muruganandham, J. Wu, Synthesis, characterization and catalytic activity of easily recyclable zinc oxide nanobundles, J. Appl. Catal. B: Environ., 80 (2008) 32–41.

[23] N. Daneshvar, D. Salari, A.R. Khataee, Photocatalytic degradation of azo dye acid red 14 in water on ZnO as an alternative catalyst to TiO$_2$, J. Photochem. Photobiol. A: Chem., 162 (2004) 317–322.

[24] A. Noraidura, A. Rusmidah, A. Wan, B. Wan Abu, G.M. Nordin, O.M. Yusuf, TiO$_2$ and ZnO on different supports for photo-degradation of paraquat, Jurnal Teknologi., 47 (2007) 1–8.

[25] M. Afzaal, M.A. Malik, P. O'Brien, Preparation of zinc containing materials, New J. Chem., 31 (2007) 2029–2040.

[26] P.V. Kamat, Meeting the clean energy demand: nanostructure architectures for solar energy conversion, J. Phys. Chem. C, 111 (2007) 2834–2860.

[27] A. Mills, J.S. Wang, M. Crow, G. Taglioni, L. Novella, Novel low-temperature photocatalytic titania films produced by plasma-assisted reactive dc magnetron sputtering, Photochem. Photobiol. A, 187 (2006) 370–376.

[28] L. Vayssieres, Growth of arrayed nanorods and nanowires of ZnO from aqueous solutions, Adv. Mater., 15 (2003) 464–466.

[29] F. Renault, N. Morin-Crini, F. Gimbert, P.M. Badot, G. Crini, Cationized starch-based material as a new ion-exchanger adsorbent for the removal of C.I. Acid Blue 25 from aqueous solutions, Bioresour. Technol., 99 (2008) 7573–7586.

[30] R. Saleh, N.F. Djaja, Transition-metal-doped ZnO nanoparticles: synthesis, characterization and photocatalytic activity under UV light, Spectrochim. Acta A: Mol. Biomol. Spectrosc., S1386–1425 (2014) 581–590.

[31] F.S. Li, H.B. Wang, L. Wang, J.B. Wang, Magnetic properties of $ZnFe_2O_4$ nanoparticles produced by a low-temperature solid-state reaction method, J. Magn. Magn. Mater., 309 (2007) 295–299.

[32] N. Ponpandian, A. Narayanasamy, Influence of grain size and structural changes on the electrical properties of nanocrystalline zinc ferrite, J. Appl. Phys., 92 (2002) 2770–2778.

[33] M.P. Pileni, Magnetic fluids: fabrication, magnetic properties, and organization of nanocrystals, Adv. Funct. Mater., 11 (2001) 323–336.

[34] X.Y. Li, Y. Hou, Q.D. Zhao, L.Z. Wang, A general, one step and template-free synthesis of sphere-like zinc ferrite nanostructures with enhanced photocatalytic activity for dye degradation, J. Colloid Interface Sci., 358 (2011) 102–108.

[35] S.W. Cao, Y.J. Zhu, G.F. Cheng, Y.H. Huang, Preparation and photocatalytic property 628 of α-Fe_2O_3 hollow core/shell hierarchical nanostructures, J. Phys. Chem. Solids, 71 (2010) 1680–1683.

[36] Y.S. Fu, X. Wang, Magnetically separable $ZnFe_2O_4$–graphene catalyst and its high photocatalytic performance under visible light irradiation, Ind. Eng. Chem. Res., 50 (2011) 7210–7218.

[37] X.Y. Li, Y. Hou, Q.D. Zhao, W. Teng, X.J. Hu, G.H. Chen, Capability of novel $ZnFe_2O_4$ nanotube arrays for simulated-sunlight induced degradation of 4-chlorophenol, Chemosphere, 82 (2011) 581–586.

[38] G.L. Fan, Z.J. Gu, L. Yang, F. Li, Nanocrystalline zinc ferrite photocatalysts formed using the colloid mill and hydrothermal technique, Chem. Eng. J., 155 (2009) 534–541.

[39] R. Comparelli, E. Fanizza, M.L. Curri, P.D. Cozzi, G. Mascolo, A. Agostiano, UV-induced photocatalytic degradation of azo dyes by organic-capped ZnO nanocrystals immobilized onto substrates, Appl. Catal., B60 (2005) 1–11.

[40] L.W. Zhang, H.Y. Cheng, R.L. Zong, Y.F. Zhu, Photocorrosion suppression of ZnO nanoparticles via hybridization with graphite-like carbon and enhanced photocatalytic activity, J. Phys. Chem. C, 113 (2009) 2368–2374.

[41] H.B. Fu, T.G. Xu, Y.F. Zhu, Photocorrosion inhibition and enhancement of photocatalytic activity for ZnO via hybridization with C60, Environ. Sci. Technol., 42 (2008) 8064–8069.

[42] Z.C. Wang, Splendid one-dimensional nanostructures of zinc oxide: a new nanomaterial family for nanotechnology, ACS Nano, 2 (2008) 1987–1992.

[43] L. Xu, Y. Au, C. Pelligra, C. Chen, L. Jin, H. Huang, S. Sithambaram, M. Aindow, R. Joeshon, S.L. Suib, ZnO with different morphologies synthesized by solvothermal methods for enhanced photocatalytic activity, Chem. Mater., 21 (2009) 2875–2885.

[44] J. Tian, Z. Wu, Z. Liu, C. Yu, K. Yang, L. Zhu, W. Huang, Y. Zhou, Low-cost and efficient visible-light-driven $CaMg(CO_3)_2@Ag_2CO_3$ microspheres fabricated via an ion exchange route, Chinese J. Catal., 38 (2017) 1899–1908.

[45] J. Tian, R. Liu, Z. Liu, C. Yu, M. Liu, Boosting the photocatalytic performance of Ag_2CO_3 crystals in phenol degradation via coupling with trace N-CQDs, Chinese J. Catal., 38 (2017) 1999–2008.

[46] H. He, S. Xue, Z. Wu, C. Yu, K. Yang, G. Peng, W. Zhou, D. Li, Sonochemical fabrication, characterization and enhanced photocatalytic performance of Ag_2S/Ag_2WO_4 composite micro-rods, Chinese J. Catal., 37 (2016) 1841–1850.

[47] D. Zeng, K. Yang, C. Yu, F. Chen, X. Li, Z. Wu, H. Liu, Phase transformation and microwave hydrothermal guided a novel double Z-scheme ternary vanadate heterojunction with highly efficient photocatalytic performance, Appl. Catal. B: Environ., 237 (2018) 449–463.

[48] S. Song, Y. Xiaoyan, Z. Yi, Z. Fan, D. Jianjun, B. Jun, G. Chen, Enhanced photocatalytic activity of sponge-like $ZnFe_2O_4$ synthesized by solution combustion method, Prog. Nat. Sci.: Mater. Int., 22 (2012) 639–643.

[49] J. Theerthagiri, R.A. Senthil, P. Arunachalam, M.H. Buraidah, J. Madhavan, S. Amutha, A.K. Arof, Synthesis of various carbon incorporated flower-like MoS_2 microspheres as counter electrode for dye-sensitized solar cells, J. Solid State Electrochem., 21 (2017) 581–590.

[50] F. Ansari, M.S. Niasari, Simple sol-gel auto-combustion synthesis and characterization of lead hexaferrite by utilizing cherry juice as a novel fuel and green capping agent, Adv. Powder Technol., 27 (2016) 2025–2031.

[51] F. Ansari, A. Sobhani, M.S. Niasari, Green synthesis of magnetic chitosan nanocomposites by a new sol–gel auto-combustion method, J. Magn. Magn. Mater., 410 (2016) 27–33.

[52] F. Ansari, A. Sobhani, M.S. Niasari, $PbTiO_3/PbFe_{12}O_{19}$ nanocomposites: green synthesis through an eco-friendly approach, Composites Part B, 85 (2016) 170–175.

[53] M. Mahdiani, A. Sobhani, F. Ansari, M.S. Niasari, Lead hexaferrite nanostructures: green amino acid sol–gel auto-combustion synthesis, characterization and considering magnetic property, J. Mater. Sci.: Mater. Electron., 28 (2017) 17627–17634.

[54] F. Ansari, A. Sobhani, M.S. Niasari, Simple sol-gel synthesis and characterization of new $CoTiO_3/CoFe_2O_4$ nanocomposite by using liquid glucose, maltose and starch as fuel, capping and reducing agents, J. Colloid Interface Sci., 514 (2018) 723–732.

[55] M. Mahdiani, F. Soofivand, F. Ansari, M.S. Niasari, Grafting of $CuFe_{12}O_{19}$ nanoparticles on CNT and graphene: eco-friendly synthesis, characterization and photocatalytic activity, J. Clean. Prod., 176 (2018) 1185–1197.

[56] M.S. Niasari, F. Soofivand, A.S. Nasa, M.S. Arani, A.Y. Faal, S. Bagheri, Synthesis, characterization, and morphological control of $ZnTiO_3$ nanoparticles through sol-gel processes and its photocatalyst application, Adv. Powder Technol., 27 (2016) 2066–2075.

[57] D. Abbasi, M.S. Ghanbari, M. Niasari, M. Hamadanian, Photo-degradation of methylene blue: photocatalyst and magnetic investigation of Fe_2O_3–TiO_2 nanoparticles and nanocomposites, J. Mater. Sci.: Mater. Electron., 27 (2016) 4800–4809.

[58] J. Theerthagiri, R.A. Senthil, A. Priya, J. Madhavan, M. Ashok-kumar, Synthesis of visible-light active V_2O_5/g-C_3N_4 composite photocatalyst, New J. Chem., 39 (2015) 1367–1374.

[59] J. Ok-Sang, H. Tae Eun, J. Euh Duck, W. Mi Sook, K. Hyunmin, Synthesis of zinc ferrite and its photocatalytic application under visible light, J. Korean Phys. Soc., 54 (2009) 204–208.

[60] R. Bangxing, H. Ying, H. Changseok, N. Mallikarjuna, D. Dionysios, Ferrites as photocatalysts for water splitting and degradation of contaminants, ferrites and ferrates: chemistry and applications in sustainable energy and environmental remediation, Chapter 3, ACS Symp. Ser., 1238 (2016) 79–112.

[61] G. Xin, L. Xiangxuan, Z. Zuoming, W. Xuanjun, X. Zheng, Enhanced photoelectrochemical and photocatalytic behaviors of MFe_2O_4 (M = Ni, Co, Zn and Sr) modified TiO_2 nanorod arrays, Sci. Rep., 6 (2016) 1–11.

[62] F. Peng, Q. Jun, H. Jin-xian, L. Jian-hong, Z. Ming, S. Bi-tao, Barium (II)-doped zinc ferrite-reduced graphene oxide nanohybrids for superior adsorption and magnetic properties, New Carbon Mater., 32 (2017) 402–410.